Microsc. Microanal. 19, S5, 89–94, 2013
doi:10.1017/S1431927613012403

Transmission Electron Microscopy Characterization of Thermomechanically Treated Al_3Ti–(8, 10, 15)% Cr Intermetallics

Ok Jun Jang, Cheol-Woong Yang, and Dong Bok Lee*

School of Advanced Materials Science & Engineering, Sungkyunkwan University, Suwon 440-746, South Korea

Abstract: The ordered $L1_2$-type Al_3Ti–(8, 10, 15)% Cr intermetallic compounds, namely, $Al_{67}Ti_{25}Cr_8$, $Al_{66}Ti_{24}Cr_{10}$, and $Al_{59}Ti_{26}Cr_{15}$, were prepared by induction melting followed by thermomechanical treatment. Their microstructure, compositional variation, and crystal structure were characterized using X-ray diffraction, optical microscopy, and scanning and transmission electron microscopy equipped with energy-dispersive spectroscopy. The $Al_{67}Ti_{25}Cr_8$ alloy consisted of the $L1_2$-Al_3Ti matrix and precipitates of α_2-Ti_3Al, $D0_{22}$-Al_3Ti, and γ-TiAl. The $Al_{66}Ti_{24}Cr_{10}$ and $Al_{59}Ti_{26}Cr_{15}$ alloys consisted of the $L1_2$-Al_3Ti matrix and grains of α-TiAl and β-Cr.

Key words: titanium trialuminides, chromium, phase diagram, intermetallics, transmission electron microscopy, energy-dispersive spectrometry

Introduction

The ordered intermetallic compounds of Al_3Ti have attracted strong interest as potential high-temperature structural materials owing to their low density, high temperature, strength, and excellent oxidation resistance. They are, however, extremely brittle at room temperature because of the low symmetry of their tetragonal $D0_{22}$ structure with few slip systems, posing difficulties in deformability. To overcome this shortcoming, Cr was added to transform the $D0_{22}$ into the cubic-ordered $L1_2$ structure with high symmetry. The $L1_2$-type Al_3Ti–Cr compounds have the necessary five independent slip systems required for homogeneous deformation. Their mechanical (Nic et al., 1992; Klansky et al., 1994; Kumar & Brown, 1996; Mabuchi et al., 1997), oxidation (Parfitt et al., 1991), and physical properties, including the phase equilibria and phase identification (Nic et al., 1992; Nakayama & Mabuchi, 1993; Klansky et al., 1994; Jewett et al., 1996; Mabuchi et al., 1997; Xu et al., 1997; Stein et al., 2001; Lee et al., 2003), have been investigated.

The formation of ternary $L1_2$-type Al_3Ti alloys and the identification of structure and phases in the Al–Ti–Cr alloys were studied for the specimens prepared via the arc-melting (Nic et al., 1992; Nakayama & Mabuchi, 1993; Klansky et al., 1994; Jewett et al., 1996; Mabuchi et al., 1997; Xu et al., 1997; Lee et al., 2003) or powder metallurgical routes (Nakayama & Mabuchi, 1993; Mabuchi et al., 1997) followed by homogenization treatment. Conventional heat treatment, however, introduced several second phases surrounding the $L1_2$ phase and porosities (Nic et al., 1992; Nakayama & Mabuchi, 1993; Klansky et al., 1994; Jewett et al., 1996; Mabuchi et al., 1997; Lee et al., 2003). With regard to the Al-rich corner of the Ai–Ti–Cr ternary-phase diagram, only a limited number of systematic studies are available. Phase equilibria in the Al–Ti–Cr system are poorly understood because of the complexity of the phase relations. Nic et al. established a partial isothermal section at 1,200°C (Nic et al., 1992; Klansky et al., 1994). Mabuchi and colleagues studied partial isothermal sections at 1,000 and 1,150°C using arc-melted and homogenized samples, as well as sintered and air-quenched samples (Nakayama & Mabuchi, 1993; Mabuchi et al., 1997). Jewett et al. (1996) studied phase equilibria involving the $L1_2$-Al_3Ti and reported partial isothermal sections at 800 and 1,000°C using arc-melted and homogenized samples. Xu et al. (1997) studied the phase equilibria of the Al–Ti–Cr system at 1,150°C by means of a diffusion triple technique. However, the information available for the Al–Ti–Cr system is far from sufficient. Most of the previous studies were conducted using X-ray diffraction (XRD), optical microscopy (OM), and scanning electron microscopy (SEM) in conjunction with energy-dispersive spectrometry (EDS), and sometimes using electron probe microanalysis (Nic et al., 1992; Nakayama & Mabuchi, 1993; Klansky et al., 1994; Kumar & Brown, 1996; Jewett et al., 1996; Mabuchi et al., 1997; Xu et al., 1997).

In this study, the Cr contents were varied from 8, 10 to 15% in order to study the phase change with Cr in the Al_3Ti alloys. The compositions denoted in this paper are all in atomic percentage. These Al_3Ti–Cr samples were induction melted, homogenized, and isothermally forged for microstructural control. This thermomechanical treatment enabled a nearly equiaxed microstructure to be obtained through dynamic recrystallization and minimized preexisting pores and second phases. The aim of this study was to characterize the phases present in the thermomechanically treated Al_3Ti–(8, 10, 15)% Cr intermetallics mainly by utilizing transmission electron microscopy (TEM). This has a high spatial resolution to ensure an accurate and reliable phase identification of the minor phases in the $L1_2$ matrix.

*Corresponding author. E-mail: dlee@skku.ac.kr

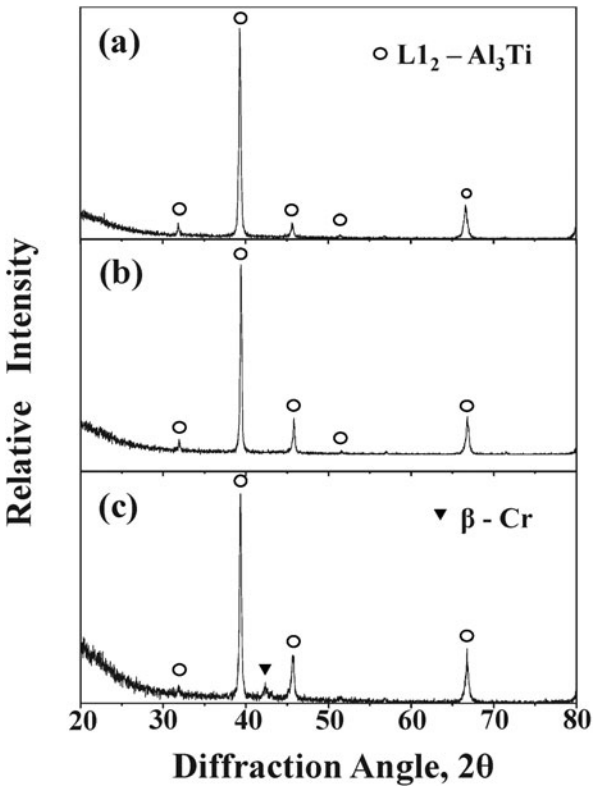

Figure 1. X-ray diffraction patterns of (**a**) $Al_{67}Ti_{25}Cr_8$, (**b**) $Al_{66}Ti_{24}Cr_{10}$, and (**c**) $Al_{59}Ti_{26}Cr_{15}$ alloys.

XRD, OM, and SEM/EDS were also utilized to characterize the microstructure, crystal structure, and composition of the alloys. TEM studies on thermomechanically treated Al_3Ti intermetallics have not been adequately performed yet, and hence this study would be a useful contribution to the literature.

Materials and Methods

Three kinds of L1$_2$-type Al_3Ti–(8, 10, 15)% Cr ingots, namely, $Al_{67}Ti_{25}Cr_8$, $Al_{66}Ti_{24}Cr_{10}$, and $Al_{59}Ti_{26}Cr_{15}$, were prepared by induction melting pure elemental stocks (Ti = 99.9%, Al = 99.99%, Cr = 99.95% in purity) in an argon atmosphere using zirconia crucibles and tilt-pouring the molten metal into a graphite mold. The ingots were heated at 1,100°C for 7 days in vacuum for homogenization; they were then furnace cooled and sectioned to sizes of 25 × 30 × 40 mm^3. These blocks were then forged in three steps in three mutually perpendicular directions to form pancakes with a thickness of ~10 mm. The forging was performed at 1,100°C for the first and second steps and at 1,000°C for the third step in an argon atmosphere with identical strain rates of $10^{-3.5}$ s^{-1}. The thermomechanically treated pancakes were cut into small test coupons, ground, and polished.

The microstructures, crystal structures, and phases in the prepared alloys were characterized using OM, XRD with Cu–Kα radiation, SEM, and TEM (operated at 300 kV) equipped with EDS. Thin foils for TEM analysis were mechanically polished to a thickness of about 30 μm and then ion milled to perforation. The composition of the L1$_2$ phase and minor phases was assessed by EDS. Structural analyses were performed using a selective area diffraction pattern (SADP) from the region of interest. In order to identify phases, in conjunction with EDS and SADP analyses the primitive cell volume and reciprocal lattice height of such interfacial reaction products were calculated using the data obtained from convergent beam electron diffraction (CBED) patterns (Kim et al., 1996; Kim & Ahn, 2006) and then compared with theoretical values.

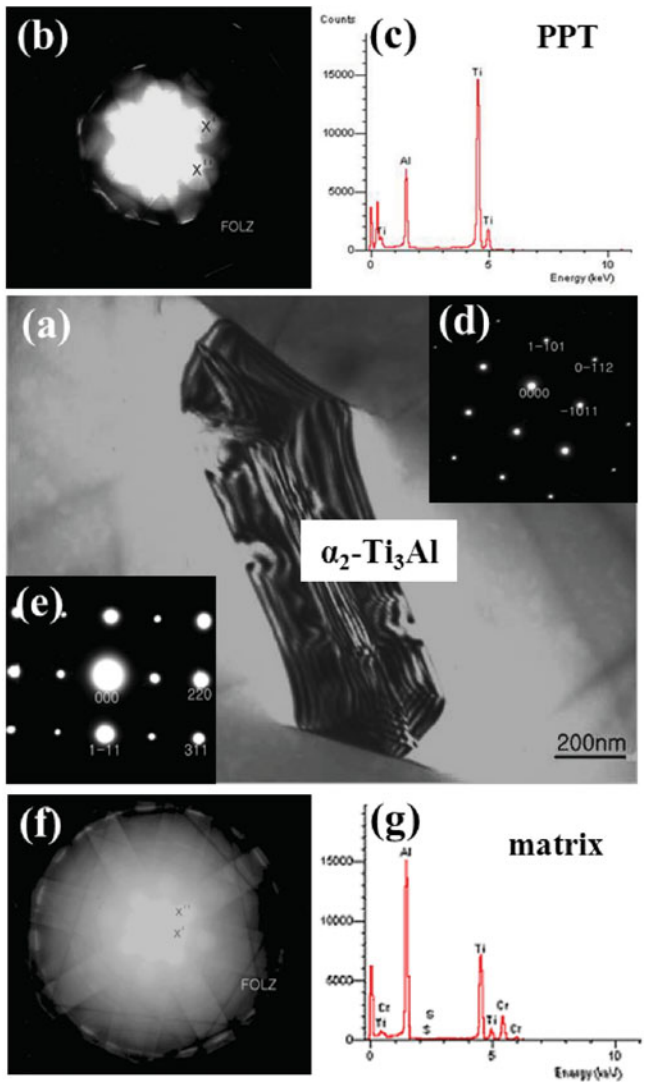

Figure 2. Transmission electron microscopy results of $Al_{67}Ti_{25}Cr_8$: (**a**) bright-field image, (**b**) convergent beam electron diffraction (CBED) pattern, (**c**) energy-dispersive spectrometry (EDS) spectrum, and (**d**) [01-11] zone axis SAD pattern of an α_2-Ti_3Al precipitate, (**e**) SAD pattern taken from [0-1-2] zone axis, (**f**) CBED pattern, and (**g**) EDS spectrum of the matrix.

Results and Discussion

Figure 1 shows the XRD patterns of the $Al_{67}Ti_{25}Cr_8$, $Al_{66}Ti_{24}Cr_{10}$, and $Al_{59}Ti_{26}Cr_{15}$ alloys. The matrix of these

https://doi.org/10.1017/S1431927613012403 Published online by Cambridge University Press

Table 1. Phases Present in $Al_{67}Ti_{25}Cr_8$, $Al_{66}Ti_{24}Cr_{10}$, and $Al_{59}Ti_{26}Cr_{15}$ Alloys According to Previous Studies and This Study.

Alloy Studied	Phase Identified by Other Studies	Phase Identified in this Study
$Al_{67}Ti_{25}Cr_8$	τ (major), Al_2Ti + Al_3Ti (minor) (Nic et al., 1992; Klansky et al., 1994) τ (Nakayama & Mabuchi, 1993; Mabuchi et al., 1997) τ (Jewett et al., 1996)	τ (major), α_2-Ti_3Al + $D0_{22}$-Al_3Ti + γ-TiAl (minor)
$Al_{66}Ti_{24}Cr_{10}$	τ (Nic et al., 1992; Klansky et al., 1994) τ (Nakayama & Mabuchi, 1993; Mabuchi et al., 1997) τ (Jewett et al., 1996)	τ (major), γ-TiAl + β-Cr (minor)
$Al_{59}Ti_{26}Cr_{15}$	τ (major), TiCrAl (minor) (Nic et al., 1992; Klansky et al., 1994) τ (major), TiAl + Cr_2Al(minor) (Nakayama & Mabuchi, 1993; Mabuchi et al., 1997) τ (major), β-Cr (minor) (Jewett et al., 1996)	τ (major), γ-TiAl + β-Cr (minor)

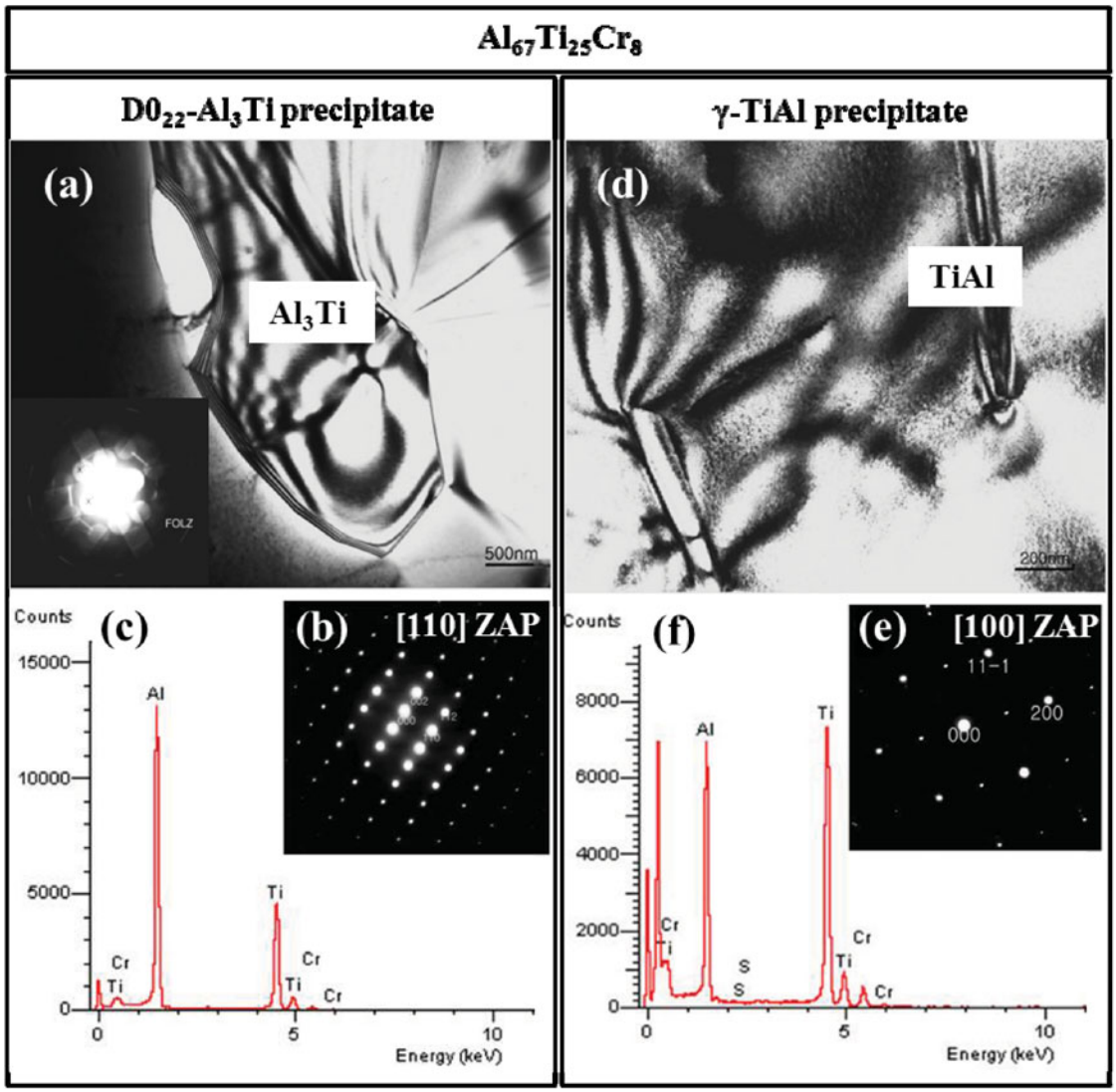

Figure 3. Various precipitates in $Al_{67}Ti_{25}Cr_8$: (**a**) transmission electron microscopy bright field (TEM BF) image, (**b**) SAD pattern taken from the [110] zone axis, (**c**) energy-dispersive spectrometry (EDS) spectrum of the $D0_{22}$-Al_3Ti precipitate, (**d**) TEM BF image, (**e**) SAD pattern taken from the [100] zone axis, and (**f**) EDS spectrum of the γ-TiAl precipitate. The inset in (**a**) shows a convergent beam electron diffraction pattern of the $D0_{22}$-Al_3Ti precipitate.

https://doi.org/10.1017/S1431927613012403 Published online by Cambridge University Press

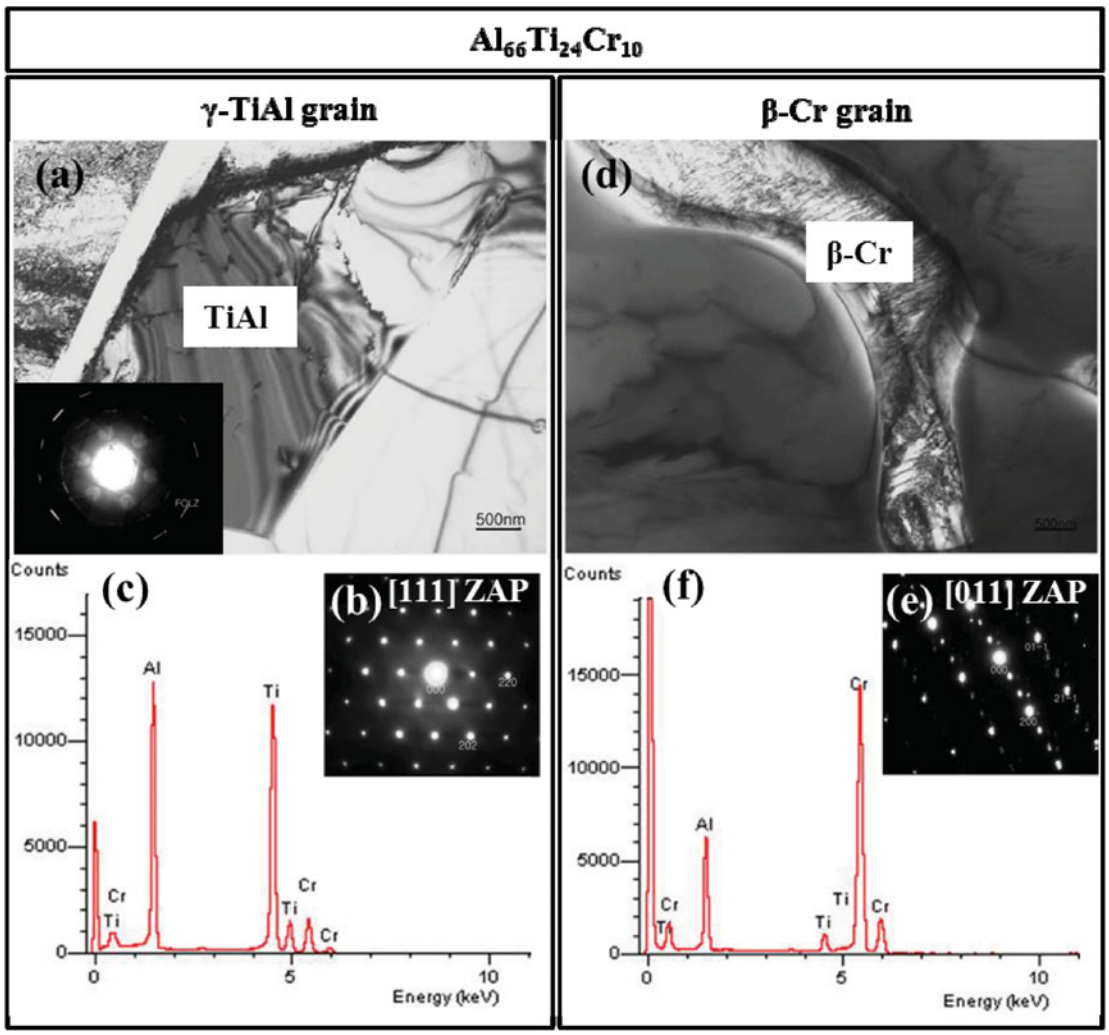

Figure 4. Transmission electron microscopy (TEM) results of $Al_{66}Ti_{24}Cr_{10}$: (**a**) bright field image, (**b**) SAD pattern taken from the [111] zone axis, (**c**) energy-dispersive spectrometry (EDS) spectrum of the γ-TiAl grain, (**d**) TEM BF image, (**e**) SAD pattern taken from the [011] zone axis, and (**f**) EDS spectrum of the β-Cr grain. The inset in (**a**) shows a convergent beam electron diffraction pattern from the γ-TiAl grain.

alloys consisted primarily of the $L1_2$-Al_3Ti phase. In addition, a small amount of the β-Cr phase was detected in Figure 1c.

Previous studies on the Al–Ti–Cr phase diagram usually focused on the $L1_2$ single phase and on the surrounding phase fields at 800–1,200°C. For example, Nic et al. (1992) reported the isothermal section of the Al-rich Al–Ti–Cr phase diagram at 1,200°C. The samples were prepared by arc-melting, homogenization with HIPing treatment (1,200°C at 172 MPa for 2 h) to minimize porosity, and slowly cooling. It is noted that the $L1_2$-Al_3Ti τ-phase coexists with six phases. Mabuchi et al. (1997) reported the isothermal section at 1,000°C. The samples were prepared by sintering at 1,000°C, followed by air quenching. In their phase diagram, the $L1_2$-Al_3Ti phase field was very narrow, with about a 1% radius and its center at $Al_{67}Ti_{25}Cr_8$. The $L1_2$ phase was surrounded by TiAl, $TiAl_2$, $D0_{22}$-Al_3Ti, $Al_{17}Cr_9$, and Cr_2Al intermetallic compounds. However, these results were obtained in a nonequilibrium manner, because the heat treatment was too short to reach equilibrium (Jewett et al., 1996; Xu et al., 1997). Jewett et al. (1996) reported the isothermal section at 800°C. This is based on the samples that were arc-melted, homogenized at 1,140–1,270°C for 3–4 h, annealed at 800–1,000°C for 100–500 h under vacuum, and water quenched. The three phase fields (τ + β-Cr + Al_8Cr_5, τ + Al_8Cr_5 + TiAl, and $TiAl_2$ +Ti(Cr,Al)$_2$ + β-Cr) were identified. Later, Xu et al. (1997) reported that the $L1_2$ phase field was much larger than that determined by Nic et al. (1992) and Mabuchi et al. (1997). It is known that the $L1_2$ phase field shifts toward the Al-rich corner of the phase diagram, and the extent of the $L1_2$ phase field decreases with decreasing temperature (Lee et al., 2003). The mismatch in composition and the stability region of the existing phases, including the $L1_2$ phase, in the Al–Ti–Cr phase diagram indicates that a lot more work needs to be done to define the Al–Ti–Cr phase diagram. The phase diagrams from the previous studies mentioned above (Nic et al., 1992; Nakayama & Mabuchi, 1993; Klansky et al.,

https://doi.org/10.1017/S1431927613012403 Published online by Cambridge University Press

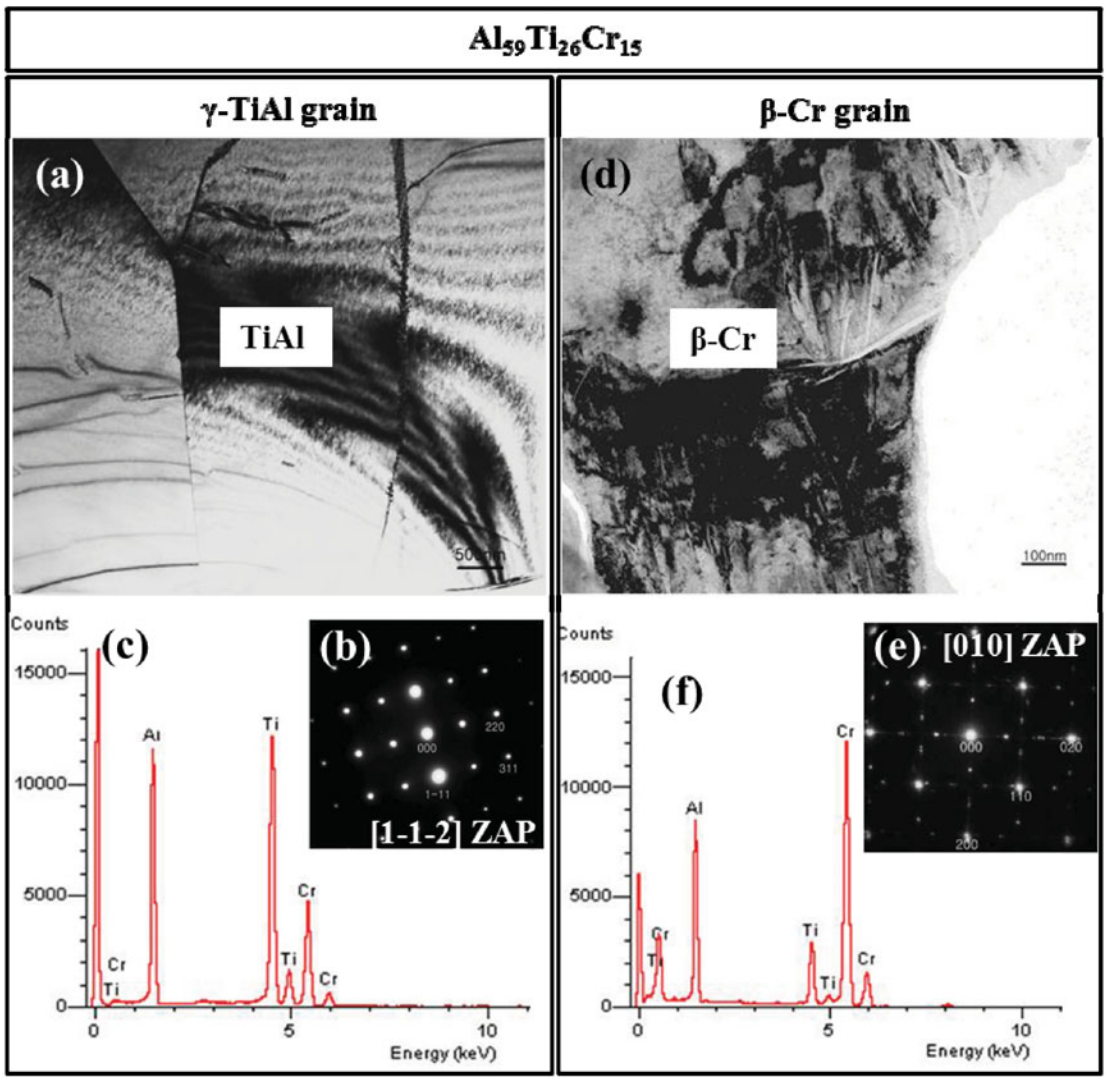

Figure 5. Transmission electron microscopy (TEM) results of $Al_{59}Ti_{26}Cr_{15}$; (**a**) bright field (BF) image, (**b**) SAD pattern taken from the [1-1-2] zone axis, (**c**) energy-dispersive spectrometry (EDS) spectrum of the γ-TiAl grain, (**d**) TEM BF image, (**e**) SAD pattern taken from the [010] zone axis, and (**f**) EDS spectrum of the β-Cr grain.

1994; Jewett et al., 1996; Mabuchi et al., 1997; Raghava, 2005) in $Al_{67}Ti_{25}Cr_8$, $Al_{66}Ti_{24}Cr_{10}$, and $Al_{59}Ti_{26}Cr_{15}$ alloys are listed in Table 1.

Figure 2a is a TEM image showing the microstructure of the $Al_{67}Ti_{25}Cr_8$ alloy. The EDS and SADP analyses of the precipitate are shown in Figures 2c and 2d, respectively. They indicate that the precipitate was α_2-Ti_3Al, whose composition was 65Ti–34Al–1Cr. From the CBED pattern of the precipitate shown in Figure 2b, the cell volume was measured as 132.36 $Å^3$ (theoretical value = 134.45 $Å^3$). The SADP and EDS spectra of the matrix are shown in Figures 2e and 2g, respectively. The matrix was confirmed as $L1_2$-Al_3Ti, whose composition was 67Al–25Ti–8Cr. The corresponding CBED pattern shown in Figure 2f indicates that the measured cell volume was 62.58 $Å^3$ (theoretical value = 62.14 $Å^3$). The phases can be identified by comparing the theoretical cell volumes and the measured data. This method is complementary to the EDS technique. The accuracy of the primitive cell determination using a CBED pattern is typically 5% with careful calibration of camera length (Kim & Ahn, 2006).

Figures 3a and 3d show the microstructure of other precipitates observed in the $Al_{67}Ti_{25}Cr_8$ alloy. The corresponding SADP and EDS analyses shown in Figure 3 indicate that the precipitate in Figure 3a was $D0_{22}$-Al_3Ti, whose composition was 75Al–24Ti–1Cr, and the precipitate in Figure 3d was γ-TiAl, whose composition was 48Ti–48Al–4Cr. The CBED pattern shown in the inset of Figure 3a indicates that the cell volume was 64.43 $Å^3$ (theoretical value = 63.74 $Å^3$). To summarize, the $Al_{67}Ti_{25}Cr_8$ alloy consisted of the $L1_2$-Al_3Ti matrix and precipitates of α_2-Ti_3Al, $D0_{22}$-Al_3Ti, and γ-TiAl, in which about 1–4% Cr was dissolved.

Figures 4a and 4d are the TEM images of the $Al_{66}Ti_{24}Cr_{10}$ alloy. The SADP and EDS analyses of the precipitates indicate that the marked grain in Figure 4a was γ-TiAl, whose composition was 51Ti–37Al–12Cr. The corresponding CBED pattern shown in the inset of Figure 4a indicates that the

https://doi.org/10.1017/S1431927613012403 Published online by Cambridge University Press

measured cell volume was 64.55 Å^3 (theoretical value = 64.01 Å^3). In addition, the grain in Figure 4d was found to be β-Cr, whose composition was 31Al–4Ti–65Cr. From SADP, EDS, and CBED analyses, the matrix was found to be $L1_2$-Al_3Ti with a composition of 63Al–27Ti–10Cr. In brief, the $Al_{66}Ti_{24}Cr_{10}$ alloy consisted of the $L1_2$-Al_3Ti matrix and γ-TiAl grains with 10%Cr and β-Cr grains with 31%Al and 4%Ti.

Figures 5a and 5d are the TEM images of the $Al_{59}Ti_{26}Cr_{15}$ alloy. The SADP and EDS analyses indicate that the marked grain in Figure 5a was γ-TiAl with a composition of 41Ti–43Al–16Cr, and the grain in Figure 5d was β-Cr with a composition of 37Al–12Ti–51Cr. From SADP, EDS, and CBED analyses, the matrix was confirmed to be $L1_2$-Al_3Ti with a composition of 59Al–28Ti–13Cr. Figure 5 indicates that the $Al_{59}Ti_{26}Cr_{15}$ alloy consisted of the $L1_2$-Al_3Ti matrix, and γ-TiAl grains having dissolved Cr and β-Cr grains having dissolved Al and Ti.

Conclusions

Three kinds of Al_3Ti–Cr alloys, namely, $Al_{67}Ti_{25}Cr_8$, $Al_{66}Ti_{24}Cr_{10}$, and $Al_{59}Ti_{26}Cr_{15}$, were prepared by induction melting followed by thermomechanical treatment. Their matrices were $L1_2$-Al_3Ti, whose compositions were (59–63)Al–(27–30)Ti–(7–11)Cr. The phases that were identified in $Al_{67}Ti_{25}Cr_8$, $Al_{66}Ti_{24}Cr_{10}$, and $Al_{59}Ti_{26}Cr_{15}$ alloys are listed in Table 1. The $Al_{67}Ti_{25}Cr_8$ alloy consisted of the $L1_2$-Al_3Ti matrix and precipitates of α_2-Ti_3Al, $D0_{22}$-Al_3Ti, and γ-TiAl. The $Al_{66}Ti_{24}Cr_{10}$ and $Al_{59}Ti_{26}Cr_{15}$ alloys consisted of the $L1_2$-Al_3Ti matrix and grains of γ-TiAl and β-Cr.

Acknowledgments

This work was supported by the Human Resource Development Project of the Korea Institute of Energy Technology Evaluation and Planning (KETEP) grant funded by the Korea Government Ministry of Knowledge Economy (No. 20114010203020).

References

Jewett, T.J., Ahrens, B. & Dahms, M. (1996). Phase equilibria involving the τ-L_{12} and $TiAl_2$ phases in the Ti–Al–Cr system. *Intermetallics* **4**, 543–556.

Kim, G.H. & Ahn, J.P. (2006). Phase identification of nano-phase materials using convergent beam electron diffraction (CBED) technique. *Korean J Microsc* **1**, 47–56.

Kim, G.H., Kim, H.S. & Kum, D.W. (1996). Simple procedure for phase identification using convergent beam electron diffraction patterns. *Microsc Res Techniq* **33**, 510–515.

Klansky, J.L., Nic, J.P. & Mikkola, D.E. (1994). Structure/property observations for Al–Ti–Cr intermetallic alloys. *J Mater Res* **9**, 255–258.

Kumar, K.S. & Brown, S.A. (1996). Response to three-point bending of the forged $L1_2$ compound $Al_{66}Ti_{25}Cr_9$. *Intermetallics* **4**, 231–244.

Lee, J.K., Oh, M.W., Oh, M.H. & Wee, D.M. (2003). Phase stability of L_{12} based alloys in Al–Ti–Cr systems. *Intermetallics* **11**, 857–865.

Mabuchi, H., Tsuda, H., Matsui, T. & Morii, K. (1997). Microstructure and mechanical properties of ternary $L1_2$ intermetallic compound in Al–Ti–Cr system. *Mater Trans JIM* **38**, 560–565.

Nakayama, Y. & Mabuchi, H. (1993). Formation of ternary $L1_2$ compounds in Al_3Ti-base alloys. *Intermetallics* **1**, 41–48.

Nic, J.P., Klansky, J.L. & Mikkola, D.E. (1992). Structure/property observations for Al–Ti–Cr alloys near the cubic $(Al,Cr)_3Ti$ phase. *Mater Sci Eng* **A 152**, 132–137.

Parfitt, L.J., Smialek, J.L., Nic, J.P. & Mikkola, D.E. (1991). Oxidation behavior of cubic phases formed by alloying aluminum-titanium (Al_3Ti) with chromium and manganese. *Scripta Metall Mater* **25**, 727–731.

Raghava, V. (2005). Al–Cr–Ti. *J Phase Equilib Diff* **26**, 349–356.

Stein, F., Zhang, L.C., Sauthoff, G. & Palm, M. (2001). TEM and DTA study on the stability of Al_5Ti_3- and h-Al_2Ti-superstructures in aluminium-rich TiAl alloys. *Acta Mater* **49**, 2919–2932.

Xu, H., Jin, Z. & Wang, R. (1997). Study on the phase equilibria of the Al–Cr–Ti system at 1050°C. *Scripta Mater* **37**, 1469–1473.